# Overview of the Aeroelastic Prediction Workshop

Jennifer Heeg [1], Pawel Chwalowski[2], Dave Schuster[3]
*NASA Langley Research Center, Hampton, Virginia, 23681*

Mats Dalenbring[4]
*Swedish Defence Research Agency FOI, Stockholm SE-16490*

**The AIAA Aeroelastic Prediction Workshop (AePW) was held in April, 2012, bringing together communities of aeroelasticians and computational fluid dynamicists. The objective in conducting this workshop on aeroelastic prediction was to assess state-of-the-art computational aeroelasticity methods as practical tools for the prediction of static and dynamic aeroelastic phenomena. No comprehensive aeroelastic benchmarking validation standard currently exists, greatly hindering validation and state-of-the-art assessment objectives. The workshop was a step towards assessing the state of the art in computational aeroelasticity. This was an opportunity to discuss and evaluate the effectiveness of existing computer codes and modeling techniques for unsteady flow, and to identify computational and experimental areas needing additional research and development. Three configurations served as the basis for the workshop, providing different levels of geometric and flow field complexity. All cases considered involved supercritical airfoils at transonic conditions. The flow fields contained oscillating shocks and in some cases, regions of separation. The computational tools principally employed Reynolds-Averaged Navier Stokes solutions. The successes and failures of the computations and the experiments are examined in this paper.**

## I. Nomenclature

| | | |
|---|---|---|
| $C_p$ | = | pressure coefficient |
| $f$ | = | frequency, Hz |
| $M$ | = | Mach number |
| $q$ | = | dynamic pressure, psf |
| $Re$ | = | Reynolds number per chord, 1/ft |
| $Re_c$ | = | Reynolds number based on wing chord |
| $V$ | = | Freestream velocity |
| $x/c$ | = | chord location, nondimensionalized by wing chord |
| $y$ | = | span-wise coordinate |
| $\alpha$ | = | angle of attack |
| $\gamma$ | = | ratio of specific heats (= 1.14 for R-134a, =1.4 for Air) |
| $(\,)_\infty$ | = | freestream value |

**Acronyms**

| | | |
|---|---|---|
| *AePW* | = | Aeroelastic Prediction Workshop |
| *BMP* | = | Benchmark Models Program |
| *BSCW* | = | Benchmark SuperCritical Wing wind tunnel model |
| *CAE* | = | Computational AeroElasticity |
| *CFD* | = | Computational Fluid Dynamics |
| *DES* | = | Detached Eddy Simulation, higher order flow solver |
| *FRF* | = | Frequency Response Function |

[1] Research engineer, Aeroelasticity Branch, Mail Stop 340, AIAA Senior Member.
[2] Research engineer, Aeroelasticity Branch, Mail Stop 340, AIAA Senior Member.
[3] NASA Technical Fellow, NASA Engineering and Safety Center, Associate Fellow, AIAA.
[4] Research engineer, Aeroelasticity Branch, Mail Stop 340, AIAA Senior Member.

*HIRENASD* = High Reynolds Number Aero-Structural Dynamics wind tunnel model
*IFASD* = International Forum on Aeroelasticity & Structural Dyanmics
*LES* = Large Eddy Simulation, higher order flow solver
*OTT* = Oscillating TurnTable
*RANS* = Reynolds-Averaged Navier Stokes, most common flow solver
*RSW* = Rectangular Supercritical Wing wind tunnel model
*RWTH* = Rheinisch-Westfaelische Technische Hochschule
*TDT* = Transonic Dynamics Tunnel
*URANS* = Unsteady Reynolds-Averaged Navier Stokes, most common flow solver

## II. Introduction

KILMARNOCK Volume contains a poem by Robert Burns[1] that nicely captures the path of the AIAA Aeroelastic Prediction Workshop (AePW). "The best-laid schemes o' mice an' men, Gang aft agley." Despite thorough discussion and wide-ranging considerations, the configurations and test cases chosen for the AePW did not always satisfy the initial intent of the organizing committee members.

The AePW[2,3,4,5] was held April 21-22, 2012 in Honolulu Hawaii, in association with the 53rd AIAA/ ASME/ ASCE/ AHS/ ASC Structures, Structural Dynamics and Materials Conference, and sponsored by the AIAA Structural Dynamics Technical Committee. The long-range goals of the AePW team are to assess the state of the art in aeroelastic computational tools and to determine future directions for code development and aeroelastic validation experiments. The direct objective of the first workshop, assessing our ability to predict unsteady aerodynamic behavior in the transonic range, came about by considering the aeroelastic problem from the perspective of validation building blocks. The workshop approach was to perform computations on configurations, exercising an array of codes, and compare the computational results with existing experimental data sets.

The workshop was held a year prior to publication of this paper. Although data comparisons and analyses are on-going, particularly regarding quantifying the HIRENASD data, this is a good point at which to assess progress. The objective of this paper is to discuss the fundamental question: What have we learned so far?

### A. Choices

The coarse-grain building blocks in aeroelasticity are: 1) unsteady aerodynamics; 2) structural dynamics; and 3) coupling between the fluid and the structure. The organizing committee members viewed the unsteady aerodynamics portion of the problem as the most challenging and the aspect that introduced the most uncertainty into an aeroelastic analysis. In the 2012 workshop, we chose to focus primarily on validating unsteady aerodynamic models and methods, with an initial venture into a weakly coupled aeroelastic system.

Within unsteady aerodynamics, the choices of smaller building blocks to include in the first workshop were driven by several criteria. The first criterion applied is the existence of a compatible and sufficient experimental data set. The second criterion applied for the initial workshop effort was perceived simplicity, both of configuration and phenomena. The flow regime was the first decision that occupied the organizing committee. The subsonic flow was thought to be well-predicted by current methods, so the choice was made to focus on the more complicated transonic regime. The intent was to have a configuration that would exhibit transonic flow, but would not contain any regions that were massively separated.

A paper authored by the organizing committee to formally kick off the workshop activity was given at the 2011 International Forum on Structural Dyanamics and Aeroelasticity (IFASD)[3]. In that paper, the choice of flow phenomena that was chosen for the first workshop intentionally avoided cases where separated flow physics dominated the problem.

> *Perhaps the most demanding aeroelastic phenomenon for unsteady aerodynamic prediction is buffet. Similar physical phenomena, including abrupt wing stall and non-synchronous vibration in turbomachinery flows, are similarly difficult to predict. In all of these cases, the aerodynamic flow itself may become unstable even in the absence of any structural motion. Once the flow becomes unstable and begins to fluctuate, it drives structural motion. Further, if the frequency of the buffeting flow coincides or nearly coincides with a structural frequency, then large structural motions may occur. Currently, buffet is perhaps the most poorly understood of all unsteady aerodynamic phenomena and thus is not a focus*

*of the present workshop, consistent with our building block approach. An aspiration of this workshop series is to assess and advance computational aeroelastic capabilities to address this complex phenomenon.*

Having said this, however, we chose a configuration and a test condition where there was suspected mild separation. Oddly, our basis for evaluating this case as having mildly separated flow turned out not to directly indicate the presence of separation, but the presence of an oscillating shock.

## III. Configurations & Test cases

Three configurations served as test cases for the AePW. Each are shown mounted in their wind tunnel test configurations in Figure 1. The Recangular Supercritical Wing (RSW) was tested in the NASA Transonic Dynamics Tunnel (TDT). A summary of the AePW results for this configuration, experimental data, configuration details and additional reference material can be found in reference 6. The Benchmark SuperCritical Wing (BSCW) was also tested in the TDT. Analyses of the experimental data set can be found in references **Error! Bookmark not defined.** and 22. Results from several of the analysts participating in the AePW can be found in references 7, 8 and 9. The High Reynolds Number Aero-Structural Dynamics (HIRENASD) model was tested in the European Transonic dynamics Windtunnel (ETW). Wind tunnel model descriptions, testing and experimental data are reported in numerous publications including references 10, 11, 12, 13 and 14. Analytical studies include the AePW results shown in references 7, 8 and 9, and in previously published studies, references 15, 16, 17, 18, and 19.

The three configurations that were chosen for the AePW all had supercritical airfoils, Figure 2, tested at transonic conditions. Each configuration was tested by actuating the model with a sinusoidal command. In the case of the RSW and BSCW, the actuation command was a pitching motion. For the HIRENASD configuration, the model was actuated using opposing sign forces applied to the top and bottom of the wing root, at the second bending mode frequency.


**a) RSW, mounted in TDT** **b) BSCW, mounted in TDT** **c) HIRENASD, mounted in ETW**

**Figure 1. Test configurations, shown mounted in the wind tunnels**

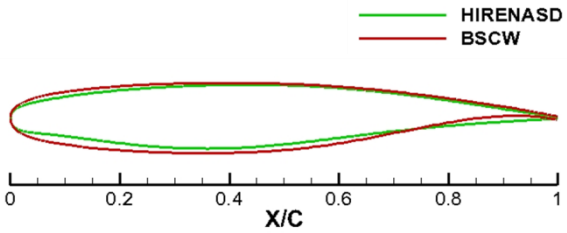


**Figure 2. Airfoil sections for BSCW and HIRENASD**

For each configuration, unforced system (steady) and forced oscillation (unsteady) analyses were performed and compared with existing experimental data sets. The unforced systems for the different configurations were treated either as rigid or flexible and analyzed with corresponding methods, as shown in Table 1. The forced systems were similarly treated, analyzed with time-accurate solutions for the unsteady flow fields. Assumed-rigid and aeroelastic systems were analyzed differently. Table 2 shows the test condition for the cases principally used in this paper for illustrating the lessons learned.

**Table 1. Solution processes for AePW configurations**

| | Unforced System | | | Forced Oscillation System, Time-accurate solutions | | |
|---|---|---|---|---|---|---|
| Configuration | Steady, Rigid | Steady, Static aeroelastic | Time-accurate, Rigid | Unsteady aerodynamic | Unsteady aerodynamics on deformed static aeroelastic mesh | Unsteady aeroelastic response |
| RSW | ✓ | | | ✓ | | |
| BSCW | ✓ | | ✓ | ✓ | | |
| HIRENASD | | ✓ | | ✓† | ✓ | ✓‡ |

† Performed only by analysis team HIRENASD-B

‡ Performed by subset of analysis teams

**Table 2. Primary test conditions and airfoil descriptions**

| Configuration | Mach | α | $Re_c$, millions | Excitation frequency, Hz | Airfoil |
|---|---|---|---|---|---|
| RSW | 0.825 | 2 | 4.01 | 10 | 12% thick airfoil modified from an 11% thick design with design point Mach 0.8, $C_L$ 0.6 |
| BSCW | 0.85 | 5 | 4.49 | 10 | SC(2)-0414 |
| HIRENASD | 0.8 | 1.5 | 7 | 80 | BAC 3-11 |

## IV. Execution

The AePW was a collaborative effort, where teams of computational fluid dynamicists applied their time-accurate aerodynamic and aeroelastic codes to common configurations. Experimentalists from Rheinisch-Westfaelische Technische Hochschule (RWTH) Aachen and NASA volunteered their data sets and made them available to the workshop committee to perform direct comparisons with the computational data sets.

Seventeen analysis teams from 10 nations participated by providing computational results for the workshop. The teams' choices of flow solvers and methodologies were left completely to their discretion, however, all teams, except two, used Unsteady Reynolds-Averaged Navier Stokes (URANS) flow solvers. The details of the grids generated and used, and flow solver parameter choices are given in reference 4.

The unforced system analyses were in general performed by converging RANS solutions to steady state. The forced oscillation simulations were performed using unsteady RANS (URANS) codes, solved in a time-accurate manner with subiterations to converge the solution at each of the time steps. Two HIRENASD analysis teams did not use RANS flow solvers. HIRENASD analysis team I performed Euler flow solutions using the ZEUS code. HIRENASD analysis team L performed full-potential flow solutions using the ST flow solver code. It should also be noted that HIRENASD analysis team C performed direct-coupled simulations rather than implementing a structural modal solver. The modal solution approach was used by all other teams in analysis of the HIRENASD case.

## V. Experiences

### A.RSW

The RSW configuration was chosen as a slam-dunk test case that didn't turn out to be that simple. The geometry of the RSW is a rectangular planform and the structure was considered to be rigid, particularly because the excitation frequencies chosen were well-below the measured structural dynamic frequencies. The complications of this configuration originate with the mounting of the model within the wind tunnel. The experimental data was obtained using an undersized splitter plate with an insufficient stand-off from the wind tunnel wall. During the AePW effort, the tunnel wall boundary layer influence on the RSW was investigated and shown to extend over a substantial portion of the wing span. The inboard row of pressure sensors, located at 31% span, was strongly influenced by the interaction with the wind tunnel wall boundary layer. The second row of pressure transducers on the wing, located at 59% span, was also shown to be significantly influenced by the tunnel wall.

In generating the computational grids, the domain was modified from the original gridding guidelines to expediently simulate the influence of the wind tunnel wall boundary layer on the wing pressure distributions. This was done by including a flat plate representation of the wind tunnel wall, modeled as a viscous surface, and subsequently tuning the upstream computational domain extent. Wind tunnel calibration data was used to determine the computational domain that produced the equivalent wind tunnel wall boundary layer thickness at the wing location. The modeling of the wind tunnel wall as a viscous surface and the change to the computational domain extent had the effect of shifting the shock forward. Reference 4 presents details of the studies that were conducted in developing this approach.

Inconsistencies introduced in resolving the wind tunnel wall issue resulted in increased scatter in the RSW computational results. This process also resulted in the specifications for the computations becoming muddied. The primary data set that was requested was the pressure distribution. Integrated loads were treated as more of an afterthought and inconsistent definitions of the integration area and normalization constants developed.

Reference 4 is intended to be a close-out report for the RSW data set. There is no detailed experimental data to plumb, no wind tunnel model to examine or retest. Analysis-only comparisons were discussed during the April 2012 workshop. Going forward, interests have shifted to analyzing the BSCW at simpler test conditions as the benchmarking point since experimental time history data and a model that can be retested are both available for this case.

### B.BSCW

Many of the computational teams had difficulty achieving a converged solution for this configuration at the AePW analysis condition, even for the unforced system case. The challenges of analyzing the BSCW model stem from the flow physics acting at the AePW test condition.

Prior to the workshop, little emphasis had been given to the details of determining solution convergence. This was one area where recommendations for improved analyses were made. In addition, the AePW analysts were given no guidelines as to whether unforced cases should be run as time-accurate or steady-state simulations. The intent was to let the physical characteristics of the problem and the observations of the individual analysts determine their simulation strategies. The chosen BSCW test cases included separated flow even under unforced conditions. All of the AePW analysts attempted steady simulations of the case with varying degrees of success. Some noted a lack of convergence in the steady simulation, but did not perform a time-accurate simulation of the unforced system, assuming that the poor convergence would be resolved in the initial transient of the subsequent forced-oscillation simulation. At least one analysis team performed a time-accurate simulation of the unforced case and demonstrated that the case produces a non-decaying unsteady separated flow character.

The experimental data, examined in detail in reference 22, is shown to contain dynamic information for the unforced system case. Some of the dynamics appear to originate as aerodynamic modes related to the separated flow over the aft portion of the airfoil. In the reference, it was determined that there are important qualitative changes introduced by the separation. Additionally, severe nonlinearities were shown to exist with respect to excitation amplitude.

These physical traits suggest that performing time-accurate solutions using higher order flow solvers should be employed for this configuration as in reference 23.

Another possibility is that, although the splitter plate is large and well-offset, there could be significant viscous interactions with the splitter plate boundary layer. One team has performed an initial investigation of this issue8. A future study, using wind tunnel data from testing the splitter plate alone for comparison is recommended.

### C.HIRENASD

The HIRENASD and associated configurations are well-documented in published literature. The HIRENASD data sets examined for AePW do not appear to contain separated flow. An evaluation of the pressure time histories at each span station rarely contains a point that indicates a shock strong enough to induce local separation. The strongest shock case is the one that will be shown in this paper, at 59% span. A local separation assessment was performed using the isentropic relationship shown in equation 1. A table of separation onset pressure coefficient values is given for the HIRENASD test medium- gaseous Nitrogen- as well as the test medium for the other two configurations. The reader can use this table to evaluate the pressure distributions published here and in the references for shock-induced separation onset.

$$C_{p,local} = \frac{2}{\gamma M_\infty^2}\left[\left(\frac{1+[(\gamma-1)/2]M_\infty^2}{1+[(\gamma-1)/2]M_{local}^2}\right)^{\frac{\gamma}{\gamma-1}} - 1\right] \quad (1)$$

**Table 3. Local shock-induced separation onset criteria**

| Freestream Mach number | Pressure coefficient for separation onset, assuming Mach 1.3 criterion | |
|---|---|---|
| | $\gamma$ = 1.4, (gaseous Nitrogen, Air) | $\gamma$ = 1.114, (R-134a, R-12) |
| 0.4 | -5.3 | -6.2 |
| 0.5 | -3.3 | -3.8 |
| 0.6 | -2.1 | -2.5 |
| 0.7 | -1.4 | -1.7 |
| 0.8 | -1.0 | -1.2 |
| 0.825 | -0.91 | -1.1 |
| 0.85 | -0.83 | -0.98 |

The HIRENASD was chosen as a first foray into aeroelastic systems. The important aeroelastic consideration to capture for the HIRENASD was found to be the static aeroelastic shape. Neither modal coupling nor excitation amplitude nonlinearities were found to be significant in the analyses.

Computational and experimental data were in better agreement for the HIRENASD configuration than for the simpler planforms. This better agreement is attributed to test conditions that produced a simpler pressure distribution for the HIRENASD model. Two test conditions at Mach 0.8 were examined during the workshop: $\alpha$ = 1.5° at 7x10$^6$ $Re_c$ and $\alpha$= -1.34° at 23x10$^6$ $Re_c$. Most example HIRENASD plots shown in this paper correspond to the first condition- it was more popular among the analysts and exhibited more dramatic behavior.

It is worth discussing why the second condition was less dramatic. The case with $\alpha$ = -1.34° was chosen because it was in an unloaded zero-lift state. It was thought that the unloaded state would be susceptible to freestream fluctuations and thus would have higher dynamic response, and would be a more challenging prediction case. This case turned out, however, to be more benign. At the zero-lift angle of attack, no upper surface shock formed. The predictions are qualitatively good on this surface. At this angle, the lower surface has more highly accelerated flow and more interesting behavior exists there. Detailed presentation of the HIRENASD data and comparisons are the subjects of future planned publications.

## VI. Data review

The data sets that are shown in this paper are a small subset of the available comparison data sets. More thorough presentations of the data are given in references 5, 6 and 22 and 20.

### A.Unforced system data

The dominant characteristic of the pressure coefficient distributions are upper surface shocks. The lower surfaces also exhibit shocks or steep pressure gradients ahead of the cusp region that characterizes supercritical airfoil geometries. The inboard span stations exhibit stronger shocks than outboard span stations, as shown in the reference publications.

The computational results agree better with the experimental data sets near the mid-span of each wing. In this region, the experimental results are relatively unaffected by the aerodynamic influences of the wind tunnel wall boundary layers and don't contain the more complicated flow structures associated with the vortices at the wing tips.

The analysis conditions chosen for all configurations were transonic- with subsonic freestream Mach numbers and supersonic regions within the flow fields. Analysis conditions were chosen where the shocks were of different strengths for the different configurations, some strong enough to promote separated flow and others weak enough that the flow was attached.

*1. Upper surface pressure distribution*

Upper surface pressure coefficient distributions for approximately equal span stations are presented for the three configurations in Figure 3. In each plot, the experimental data sets are shown by the black filled circles. Bounds on the experimental data are presented for the BSCW and HIRENASD, where time history information was available to calculate these bounds. Also shown in each plot are all of the submitted computational results for that test case, shown by the colored lines and symbols.

The shape of the upper surface pressure distribution differs greatly when comparing the three configurations. The forward portion of the distributions of the RSW and BSCW appear much flatter than the HIRENASD distribution and the upper surface shock is stronger for the first two configurations in comparison with the HIRENASD. These differences reflect the differences in the test conditions and geometry. The Mach number is lower for the HIRENASD, as is the angle of attack. Additionally, the HIRENASD is a swept wing, which lowers the Mach number normal to the shock. Finally, the airfoil geometry is substantially different, as shown in Figure 2.

The RSW upper surface pressure distribution is characterized by a flat supersonic pressure plateau ahead of the shock, a near-mid-chord shock, and an aft-of-shock pressure distribution. The shape of the aft pressure distribution includes a near-sonic plateau and a re-acceleration hump prior to the final pressure recovery at the trailing edge. The forward portion of the BSCW pressure distribution is similar to the RSW, but has slightly accelerating flow ahead of the shock, indicated by the slight up-slope of the distribution on the plot. The HIRENASD distribution is characterized by accelerating flow from the leading edge to the shock.

The HIRENASD analysis conditions also included a test case at Mach 0.8 at a negative angle of attack, -0.134°, and a test case at Mach 0.7 at 1.5°. The upper surface pressure coefficient distributions at the same span station, 59%, are shown for these two test conditions in Figure 4. Calculated results at the lower Mach number produced the best match between calculations and experiment for the workshop. At this condition, there is no shock; there are no steep pressure gradients.

*2. Trailing edge*

The trailing edge value of pressure coefficient is positive for the RSW and HIRENASD cases, indicating that the flows at the trailing edges are attached. The BSCW data set is negative at the trailing edge, indicating separated flow. There is also separated flow indicated at the foot of the shock for the BSCW configuration. Using isentropic flow relationships, the local pressure coefficient ahead of the shock violates the guideline of local Mach number being lower than 1.3 to maintain attached flow behind the shock. This guideline is based on assessment of experimental databases to determine what local Mach number corresponds to a shock of sufficient strength to separate the flow locally[21]. The other two configurations have local pressure coefficients lower than those generally required to introduce local separation.

*3. Upper surface shock*

The computational results show the upper surface shock predicted too far aft for the RSW and BSCW. The shock shape and distribution at the foot of the shock are poorly predicted. Furthermore, the variation in shock location and strength shown among the computational results is large. Towards the trailing edge, the RSW pressure distribution shape is well-predicted. The BSCW, by contrast, is not. The negative pressure coefficient at the trailing edge is discussed in reference 22 as corresponding to separated flow. The computational results do not capture this behavior.

For HIRENASD, the computations predict a shock location that is aft of the mean experimental pressure distribution. The experimental data bounds encompass all but one of the computational data sets, that set being generated with a lower order flow solver. The upper and lower bounds on the experimental data should be considered in the comparisons, rather than the mean value. As shown in other publications, the mean is not a good representation of the data in the vicinity of the shock. Future publications will focus on generating better representations of the experimental data and quantifying the differences between experiment and analysis for the

HIRENASD. Additional work is progressing to quantify the influences of analysts selections of parameters and variations introduced by different grids. However, a qualitative statement can be made saying that the computations generally capture the shape of the pressure distribution.

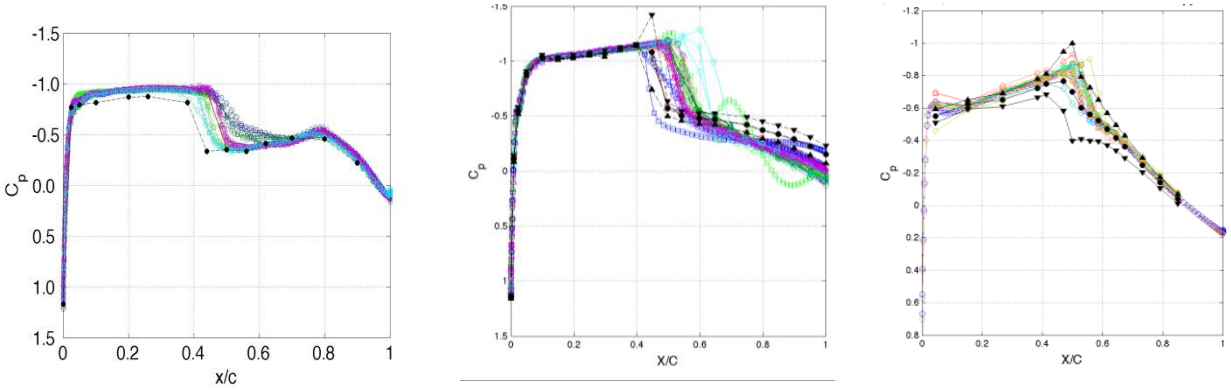


**a) RSW, station 2, 59% span ($\alpha$ = 2°, Mach = 0.825)**

**b) BSCW, 60 % span ($\alpha$=5°, Mach =0.85)**

**c) HIRENASD, station 4, 59% span, ($\alpha$ = 1.5°, Mach 0.80)**

**Figure 3. Upper surface pressure coefficient distributions, unforced system data**

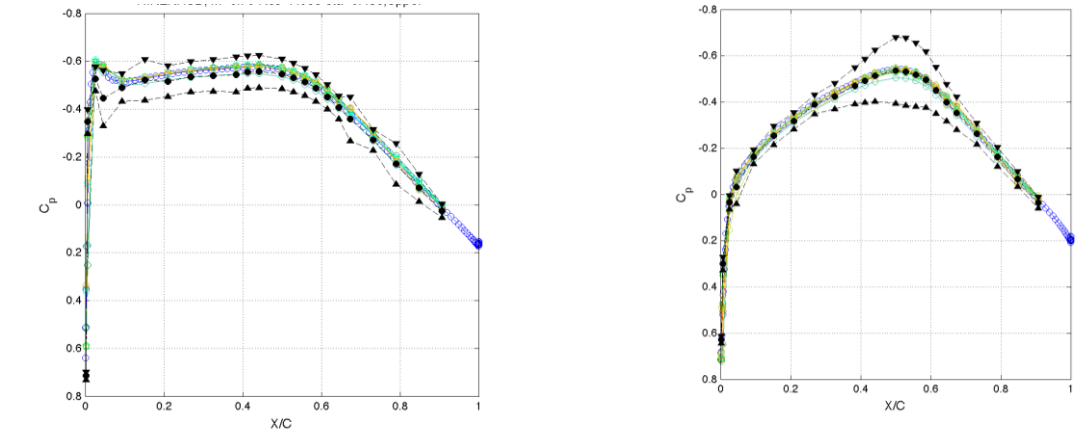


**a) Mach 0.7, $\alpha$ = 1.5°**

**b) Mach 0.8, $\alpha$ = -1.34°**

**Figure 4. HIRENASD pressure coefficient distribution, unforced system, station 4, 59% span**

*4. Lower surface*

The lower surfaces also contain shocks or at least large pressure gradients near the leading edge of the cusp regions. Harris reported than supersonic flow on the lower surface of supercritical airfoils generally resulted in separation being observed in the cusp region. The current interpretation of the AePW data is that this holds true for the BSCW, possibly for the RSW, not for HIRENASD.

On the lower surfaces, the computational results agree well with the experimental data with a few exceptions, most noticeably in the cusp regions of the RSW and BSCW. Previous publication of the RSW results detailed the boundary layer thickening- and possibly separating- in this region. The shape of the distribution is flatter than that seen in a classical supercritical airfoil pressure distribution. Over-prediction in the cusp region is more dramatically observed for the BSCW configuration. Note that the pressure coefficient change across the cusp region is much larger for the BSCW than for the other two configurations.

The other lower surface region that is anomalous is a knee in the BSCW pressure distribution at 10% chord. The physical source of this discrepancy has not been determined.

For the HIRENASD, the lower surface pressure distribution is well-predicted. The improved agreement between the experiment and computational results in the cusp region is thought to be due to the different flow

physics. Notice that this experimental data set has a concave shape over the cusp region, indicating that the flow here is attached. There are three differences that likely contribute to this qualitative difference and improved agreement. The cusp geometry of the HIRENASD airfoil section is more mild than that of the other configurations, that is, the derivative of the shape change with respect to wing chord is smaller. The HIRENASD test case is at a lower angle of attack than the other configurations. The Reynolds number for the HIRENASD case is higher, approximately 1-½ times that of the BSCW. All of these factors are such that they would tend to make the boundary layer more prone to remaining attached.

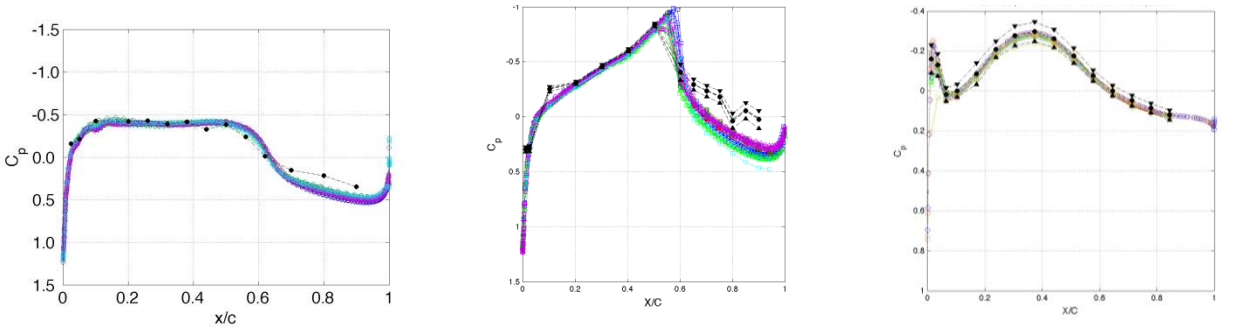


**a) RSW, station 2, 59% span (α = 2°, Mach = 0.825)**

**b) BSCW, 60 % span (α=5°, Mach =0.85)**

**c) HIRENASD, station 4, 59% span (α = 1.5°, Mach 0.80)**

**Figure 5. Lower surface pressure coefficient distributions, unforced system data**

## B. Forced oscillation data

*1. Time histories*

The experimental data for the AePW presented challenges. Where the time history data was available, it was easier to capture the important characteristics of the data set. In the case of the RSW data, only reduced data was available- mean pressures for the unforced system data and frequency response functions at the forcing frequency. This greatly hampered our ability to assess nonlinear effects. For BSCW and HIRENASD, the forced system data sets all indicate that there are nonlinearities in the pressure responses as the shock oscillates across a transducer. The data sets also show increased random components in the measurements in separated flow regions. Without the time histories for the data, this cannot be assessed. Example time histories and histograms are shown for the BSCW configuration for a sensor ahead of the shock, being crossed by the oscillating shock and in the region of separated flow aft of the shock. The character of the time histories varies significantly for these airfoil regions. Examining the histogram for the shock-crossed sensor, it is shown that the mean value is a poor representation of the most-likely value for the pressure to assume. Note the extreme left skewness in Figure 6,b,ii, indicating that the shock spends most of its time behind the transducer, a feature that can also be readily confirmed by the pressure coefficient time history. Comparison of time history data for computation and experiment will be presented in future publications.

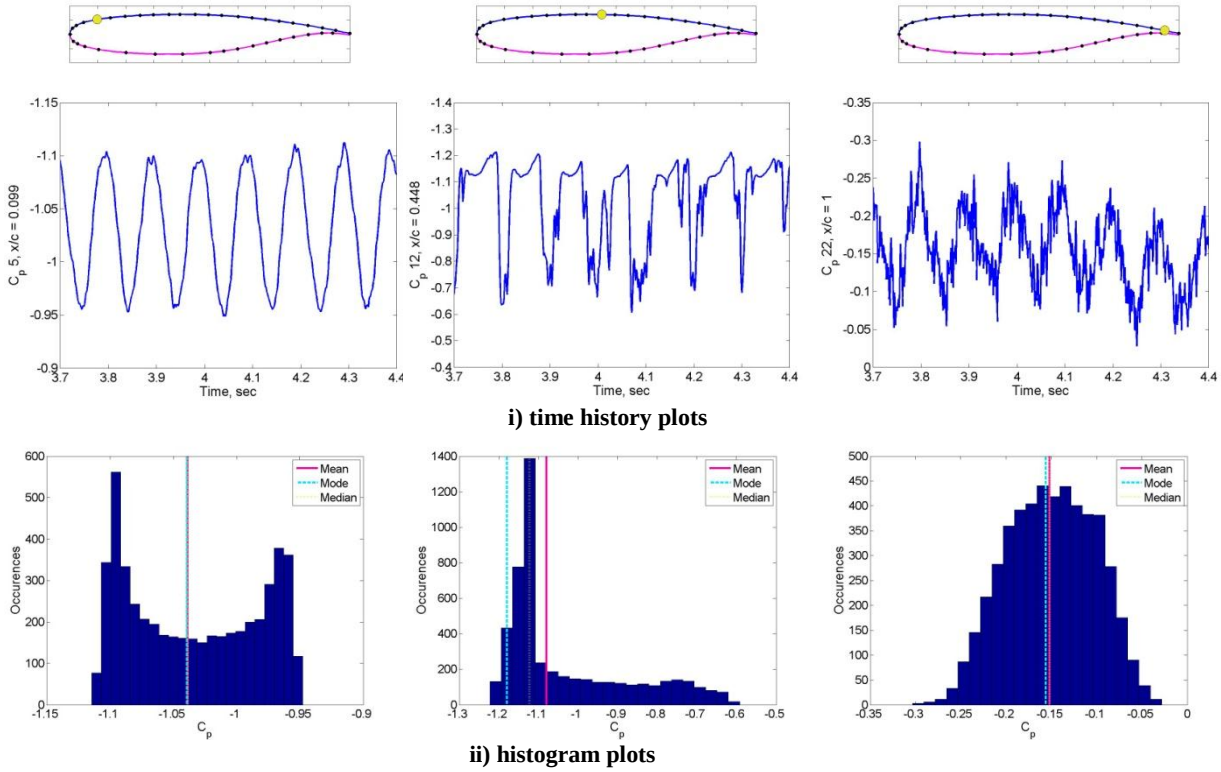


**i) time history plots**

**ii) histogram plots**

**a) Pressure transducer 5, x/c = 0.1, in region of attached turbulent flow**

**b) Pressure transducer 12, x/c = 0.45, in region of shock oscillation**

**c) Pressure transducer 22, x/c = 1.0, in separated flow region, at trailing edge**

**Figure 6. BSCW pressure coefficient behavior in different regions of the airfoil, AePW analysis condition (Mach 0.85, α 5°, 200 psf), 10 Hz forced oscillation**

*2. Frequency response functions*

Frequency response functions (FRFs) are calculated as the frequency-domain relatiobnship between the pressure coefficients and a displacement measurement. In the case of the RSW and BSW, the reference displacements are the angles of attack. For the HIRENASD, the reference displacement is the non-dimensionalized displacement at a location near the wing tip. The information shown corresponds to the FRF at a single frequency, that of the forced excitation. The result of a frequency response function calculation is a complex number that can be represented in rectangular form as real and imaginary components, as shown in reference 5, or in polar form as a magnitude and phase. The magnitude represents the ratio of the amplitude of the response quantity (pressure coefficient) to the magnitude of the reference quantity (displacement). The phase represents the time delay between the response and the reference quantity.

a. Upper surface FRFs

The FRFs for the upper surface responses are presented first in

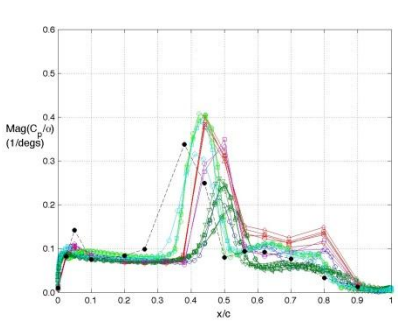


**a) RSW, station 2, 59% span ($\alpha$ = 2°, Mach = 0.825, 10 Hz excitation frequency)**

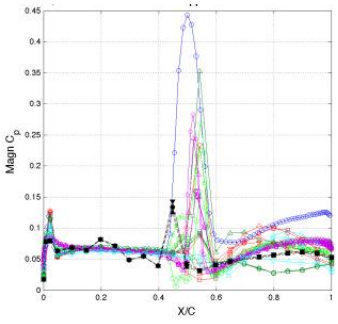


**b) BSCW, 60 % span ($\alpha$=5°, Mach =0.85, 10 Hz excitation frequency)**

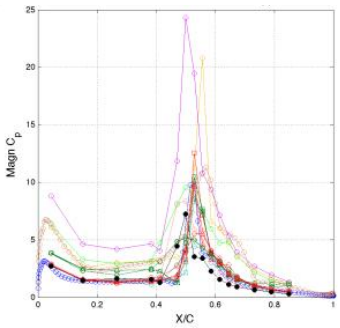


**c) HIRENASD, station 4, 59% span ($\alpha$ = 1.5°, Mach 0.80, 80 Hz excitation frequency)**

Figure 7 (magnitude) and in Figure 8 (phase). The same span station is shown for the dynamic responses as was shown for the unforced system data.

The upper surface FRFs are dominated by the shock motion, shown by the large peaks near mid-chord. The peak magnitude appears to be over-predicted by the computations, but the true peak in the experimental data is difficult to ascertain due to the transducer spacing in the vicinity of the shock. The shock motion is also generally predicted to occur further aft than shown by the experimental data.

For the RSW, none of the methods predict the peak at the proper location, reinforcing the information discussed for the unforced system prediction of the shock location. Recall that all of the computational results predict the unforced system shock further aft than the experimental data. Behind the shock, the variation in the prediction increases dramatically as compared to ahead of the shock. We interpret this increase in variation from several perspectives. For the first perspective, we revisit the discussion of the unforced system results. Within the unforced system results, there were two groupings- subsets- based on predicted shock location. Maintaining these subsets, the aft-shock-location predictions correspond to the unsteady predictions where the aft distributions lie below the experimental data. The forward-shock-location predictions correspond to the unsteady predictions where the aft distributions have larger magnitude than the experimental data. The second perspective in considering the level of variation aft of the shock focuses on the specifics of the computational modeling itself. The variation within each of the subsets are thought to show the variation of the manner in which the different computational schemes attempt to capture the shock/boundary layer interaction and the influence of the prediction of this interaction on the downstream pressure distribution.

The phase plots of the computational results in this region show consistent trends with the experimental data, indicating that the computations do a good job of predicting the time delays of the pressures in this region.

Examining all of the results as a group, it perhaps surprising that the RSW seems to be the worst-predicted case aft of the shock, since the unforced system case was determined to be an attached flow case. The likely sources of the RSW solution variation have been discussed above. This mismatch with the experimental data in this region may be strictly related to the wind tunnel wall influences. Another possible source of the mismatch is the onset of locally separated flow. The forced excitations applied to the RSW and BSCW configurations represent sinusoidal increases and decreases in the angle of attack. The angle of attack excursion to larger positive angles moves the configuration temporarily closer to or deeper into a separated flow state. In the case of the BSCW, the flow has been discussed as separated throughout the angle of attack oscillations. For the RSW, the flow is likely attaching and separating at least in the vicinity of the foot of the shock, and at the frequency of the excitation. As discussed relative to the BSCW cases, the computational methods applied fall short in predicting the separating flow effects. For the RSW case, the separation region would be very localized, which reduces the probability of its significance in these comparisons. This cannot, however, be ruled out as a contributing factor.

The BSCW shock dynamics are more poorly predicted than the other configurations. A relatively good match is shown between experiment and computations in the separated flow area in terms of the shape of the distribution, although the computations overpredict the magnitude. There are several points that should be kept in mind in interpreting these results. In this region, reference 22 shows that the coherence functions between the pressure coefficients and the angle of attack decrease, indicating that the frequency response function calculations contain more uncertainty in this region than in the forward area of the airfoil. Additionally, reference 22 showed that the influence of the separated flow was not concentrated at the excitation frequency; it is either a broad-band excitation

or concentrated at frequencies corresponding to aerodynamic modes. The time histories and frequency domain analyses presented in reference 22 show the increase in dynamics at non-excitation frequencies that are only captured in this FRF analysis as leakage effects.

For the HIRENASD, the peak spans several of the chord-wise sensors. The shape of the peak indicates that the shock is crossing one sensor, but the sensor just aft of that point also contains considerable dynamics in comparison with the RSW and BSCW. This could be due to an expanded range of the shock oscillation, better sensor locations than available for the other configurations, or dynamic separation at the foot of the shock.

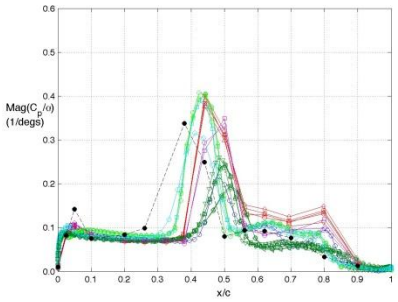


**d) RSW, station 2, 59% span (α = 2°, Mach = 0.825, 10 Hz excitation frequency)**

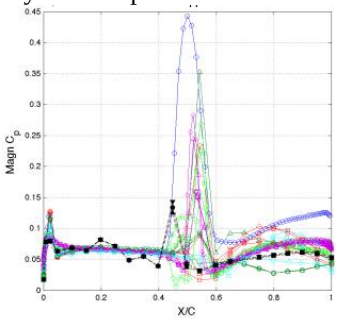


**e) BSCW, 60 % span (α=5°, Mach =0.85, 10 Hz excitation frequency)**

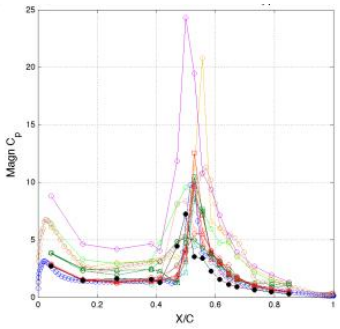


**f) HIRENASD, station 4, 59% span (α = 1.5°, Mach 0.80, 80 Hz excitation frequency)**

**Figure 7. Frequency response function magnitude, Upper surface pressure coefficient distributions due displacmeent, forced excitation data**

The phase characteristics, shown in Figure 8, indicate the different character of each of the forced oscillation cases. The BSCW case was oscillated at a frequency that can be treated as nearly quasi-static; the reduced frequency for the case shown is 0.09. The phase is principally shown in the figure at 180°, which means that the pressure coefficient and the angle of attack differ by a sign. The phase of the shock is shown to change, almost to 0, which would represent in-phase behavior, with both variables having the same sign. Given the sign conventions for each of the variables, the phase plot indicates that the shock is moving aft as the angle of attack increases. Despite the poor representation of the pressure coefficient in the region of separated flow, the computations appear to capture the sign of the shock motion. This is significant because the shock motion phase changes with the onset of separated flow, as discussed in reference 22. These two trends seem contradictory and bear further investigation.

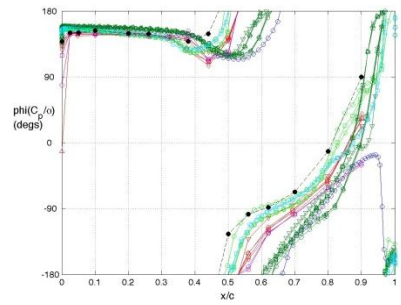


**g) RSW, station 2, 59% span (α = 2°, Mach = 0.825, 10 Hz excitation frequency)**

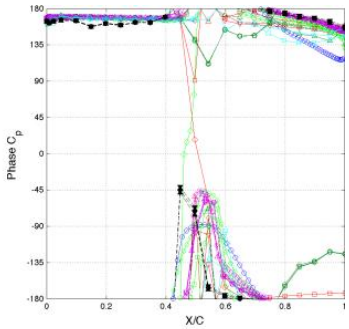


**h) BSCW, 60 % span (α=5°, Mach =0.85, 10 Hz excitation frequency)**

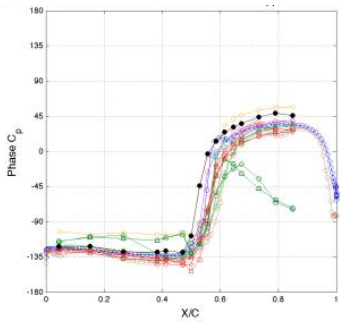


**i) HIRENASD, station 4, 59% span (α = 1.5°, Mach 0.80 80 Hz excitation frequency)**

**Figure 8. Frequency response function phase, Upper surface pressure coefficient distributions due displacement, forced excitation data**

b. Lower surface FRFs

**For the lower surface, example frequency response function magnitudes are shown in**

Figure 9 and phase plots are shown in Figure 10. Elements of the comparisons relative to the upper surface results will be highlighted.

For the BSCW, the FRF computations show a lower surface shock at 60% chord. This is at the leading edge of the cusp region. The experimental results do not show any significant dynamics in this region. During the AePW this issue was discussed and two possible scenarios were suggested: either the shock was stationary on the lower surface, or the dynamics were being missed due to the sparseness of the lower surface sensors in this region. Reference 22 showed results that illustrate that it is likely a combination of the two suggested scenarios. The location of the lower surface shock is relatively fixed; the oscillations are over a more narrow spatial range. Histograms and skewness calculations of the lower surface responses in this region, and trends with Mach number and angle of attack showed that the principal cause of the qualitative mismatch between the computations and the experiment is that the shock motion occurs for a location between two sensors. It was determined that shock dynamics exist between the two sensors at x/c = 0.5 and 0.6. Note that this interpretation of the experimental data still indicates that the computations predict the shock dynamics too far aft.

The dynamics in the cusp region for the BSCW are shown to be poorly predicted. Again, this is thought to indicate the separated flow dynamics.

The HIRENASD results show the computational results in two groups. Details of this data are the subject of ongoing studies.

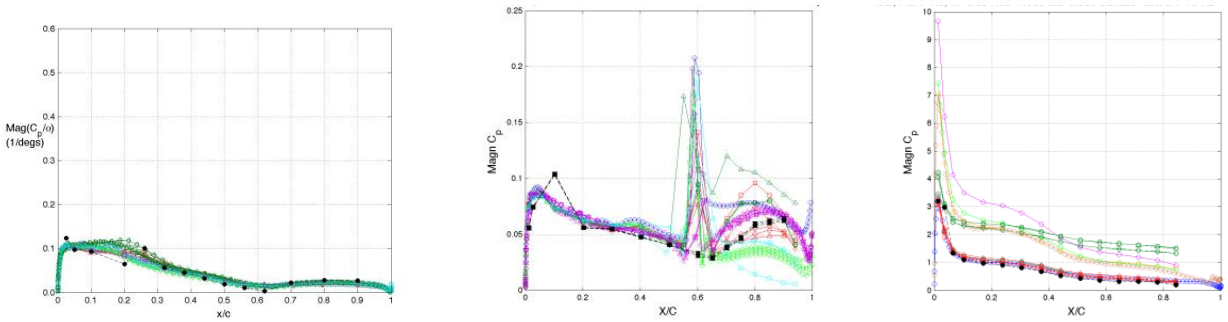


**a) RSW, station 2, 59% span (α = 2°, Mach = 0.825), 10 Hz**

**b) BSCW, 60 % span (α=5°, Mach =0.85), 10 Hz**

**c) HIRENASD, station 4, 59% span (α = 1.5°, Mach 0.80), 80 Hz**

**Figure 9. Frequency response function magnitude, Lower surface pressure coefficient distributions due displacmeent, forced excitation data**

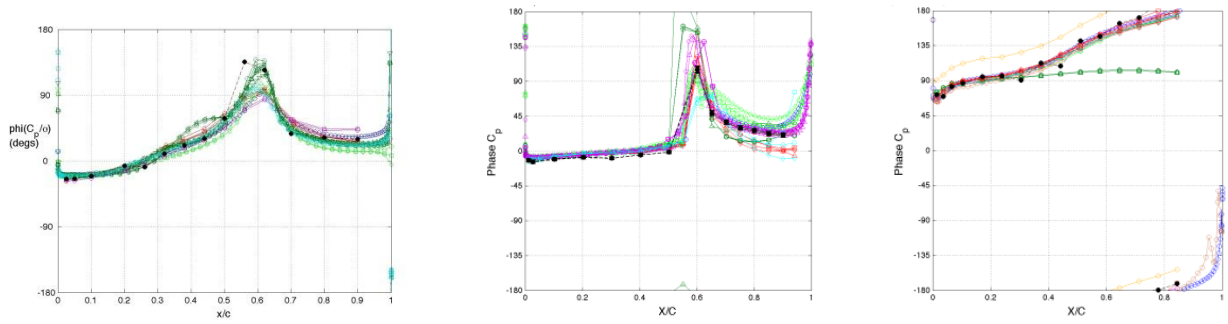


**d) RSW, station 2, 59% span (α = 2°, Mach = 0.825), 10 Hz**

**e) BSCW, 60 % span (α=5°, Mach =0.85), 10 Hz**

**f) HIRENASD, station 4, 59% span (α = 1.5°, Mach 0.80), 80 Hz**

**g)**

**Figure 10. Frequency response function phase, Lower surface pressure coefficient distributions due displacmeent, forced excitation data**

## VII. What have we learned to date?

The workshop effort utilized existing experimental data sets to validate or benchmark aspects of computational aeroelasticity tools. The workshop was structured to address the following questions.

- How good are our tools, and what aspects of those tools need further development?
- Given the comparisons that we were able to make, what comparison data or experimental data characteristics would have improved our confidence in experiment representing relevant truth? Through the exercise of existing data sets, the workshop team also sought to identify requirements for additional validation experiments by further defining what constitutes a "good validation data set" for computational aeroelasticity.

Many of the following points have been illustrated in the presentation and discussion of the limited data set. Details pertinent to other points will require that you read the supporting references. The following questions are listed and answered to the best of our ability at this point. As analysis of the data sets continues, we hope to update this information, increasing its value for future efforts.

- What were the most challenging aspects regarding our chosen configurations? What were the consequences of these aspects?
    - Each of the principal test conditions for these configurations contained an oscillating upper surface shock, and in some cases a lower surface shock. The largest magnitude of the dynamics, i.e. in the FRFs, is the shock oscillation. For forced oscillation cases, the shock oscillation follows the forcing function and responds primarily at that frequency.
    - The most challenging aspect of the RSW configuration was introduced by the promixity of the model to the wind tunnel wall and the undersized splitter plate. The consequence of attempting to capture the wall influences was that the CFD solutions varied widely, even for the unforced system results. We don't currently view the variation present in these results as an accurate assessment of the variation introduced by analysts' choice applicable to the state of the art.
    - Shock-induced separated flow and trailing edge separation was present for the BSCW configuration at our selected test conditions. Lower surface separation in the cusp region was also likely to have occurred. The computational methods had difficulty producing converged solutions for the unforced system and for the lower frequency forced oscillation case. We have attributed the convergence problems of these solutions with the complexity of the flow field.
    - HIRENASD was not as challenging as the simpler geometries of the RSW and BSCW due to test condition selection and airfoil geometry. The resulting flow physics were more easily captured by the flow solvers chosen. The zero-lift case, chosen with the thought that the shock would be less stationary, offered less of a challenge to analysts than the test case with an upper surface shock.

- What have we learned about the state of the art in aeroelastic computations?
    - Using RANS, we cannot accurately capture separated flow associated with the BSCW at the chosen test conditions. Although the test case was thought to contain moderately separated flow, the region of separation appears to extend from the mid-chord (shock location) to the wing trailing edge. Further, the dynamics of the flow are of essential interest in our studies. While RANS solutions may be able to predict an averaged influence of separation for small separation bubbles, they appear insufficient for either the unforced or forced oscillation responses of the BSCW configuration at Mach 0.85, $\alpha$=5°.
    - Grid refinement was not shown to improve correlation with experimental data for any of the configurations. For HIRENASD, preliminary indications are that the grid refinement did, however, reduce the variation in the predictions.
    - Time step refinement was not systematically investigated by many analysts. In the few cases where it was examined and separated flow was present, qualitative changes in the results were observed.

- Modeling inconsistencies may have been responsible for the large variations observed in both the unforced system response and the frequency response functions.

- What have we learned regarding flow solvers?
  - The computational fluid dynamicists generally chose RANS flow solvers, and the majority chose to use either a Spalart-Allmaras turbulence model or Menter's Shear Stress Transport turbulence model. These choices reflect the state-of-the-art or perhaps, better-phrased, the state-of-the-current practices within the CFD community. In terms of common practice for aeroelastic solutions, this represents the practices of those on the leading edge of modeling complexity. This level of flow solution is perhaps becoming more common, however, linear methods such as doublet lattice aerodynamics and ZONA are still more commonly used by practitioners.
  - In cases without large separated flow regions or significant wind tunnel wall boundary layer effects, the RANS computational methods capture qualitative features for these fairly thick supercritical airfoils. The scatter among the results is surprisingly large where vicsous effects are significant. In the cases where separated flow or geometrically-thickened boundary layers are indicated by the experimental data, these methods appear to qualitatively mis-predict even the steady pressure distributions. The HIRENASD compared better with experimental data than the other two configurations, attributable to the lack of separated flow in the HIRENASD experimental data. This qualitative difference in the flow field is assessed to be due to the less severe airfoil geometry and angle of attack.
  - Performing time-accurate solutions for unforced systems may be necessary. Paying attention to convergence of dynamic quantities with respect to time step size is recommended. The time-accurate solutions using RANS, however, have led to consideration that higher order flow solvers may be required to capture the aerodynamic source of the excitation.
  - Flow solutions that offer better fidelity in capturing turbulence, such as LES or DES, have generally been recommended in the literature for analyzing cases "massively separated flows" exist, usually occurring at high angles of attack. The highest mean angle of attack case for the AePW was the BSCW configuration, $\alpha = 5^{o}$. This test case generated what was assessed as moderately separated flow. The workshop results for BSCW led to the assessment that the URANS solutions were insufficient for this case. Some analysts are pursuing higher order CFD methods for this configuration[23]. In this case, at a moderate angle of attack, the separated flow features are significant enough to cause a qualitative change to the shock motion and qualitative changes in the aft loading. While these changes may or may not be significant for integrated loads such as lift and pitching moment coefficient, they are likely significant for assessing aeroelastic stability, which is highly dependent on phase relationships and load distribution.
  - In order to get the steady pressure distribution correct, it is essential to get the static aeroelastic deformed shape correct. Failure to do this results in effective changes in the angle of attack. Using the rigid shape, rather than the deflected aeroelastic shape resulted in overprediction of the pressure distribution.
  - Convergence criteria and subiteration criteria are not uniformly applied. Each analyst chooses their own criteria and seems to be pretty defensive about it.
  - Methodologies for analyzing unsteady oscillatory response are not standardized. Several methods were employed, although it has not been assessed whether the difference in oscillation method was a substantial source of variations observed.
  - Analysis teams almost universally chose to build their own grids, leading to uncertainties and variations associated with interpreting the gridding guidelines. Most analysts, when asked, simply said that it was easier for them to build their own grid rather than translating an existing grid.

- What have we learned regarding experimental data?
  - "Steady" is a misnomer, particularly in the case of experimental data, but also perhaps in the case of computational data. The "steady" data was acquired from wind tunnel models that

were sitting in the freestream turbulent wind tunnel flow field. These unforced systems generated data that contained oscillatory shock motion, oscillating regions of separated flow, influences of structural dynamic and facility aerodynamic modes.
    - Using the mean value to capture a pressure distribution where there is an oscillatory shock results in smearing, canting and magnitude reduction of the pressures in the region of the shock. Mean value representations even for the unforced system should incorporate maximum and minimum bounds if nothing more descriptive.
    - A validation data set should contain repeat data points and small intentional variations of test parameters such as Mach, angle of attack and Reynolds number.
    - An ideal data set would contain simultaneous measurements of structural deformation, integrated loads, unsteady pressures, skin friction coefficients, and off-body flow fields.
    - Time-domain data for presumably steady tests should be acquired and saved.
    - Wind tunnel wall boundary layer interactions may dominate a data set if the experiment is not properly designed. Measurement of facility boundary pressures and accelerations should be considered in any benchmarking test.

- What have we learned regarding postprocessing of computational data?
    - The amount of information generated in performing an unsteady CFD calculation is generally insufficient for performing computations when the frequency of the response is not exactly known and exactly captured in an integer number of data samples. Fourier analysis of linear system responses are fine and the number of cycles does not have to be excessive.
    - Typically, computational solutions are not run for a sufficient amount of time to utilize classical techniques for assessing and reducing the errors in the Fourier coefficients.
    - The data processing for CFD data is significantly different from classical experimental data processing. It is much more reminiscent of processing signals generated from a multisine signal. The results are highly sensitive to exactly capturing single cycles and setting the Fourier block size to match.
    - Classical Fourier analysis techniques may not be sufficient for analysis of CFD data that consists of limited sample sizes and short time records. New techniques that can be equally applied to both CFD and experimental data should be investigated.

- What did we learn about test case selection?
    - There were too many test cases in this workshop. The number of configurations- 3- diluted the potential lessons learned for any single configuration, and made it exhausting for the analysis teams.
    - Have a benchmark test case. While choosing a challenging case is a good thing, choosing a first test condition for putting a stake in the sand is essential. In mid-analysis cycle we added the Mach 0.7 case for the HIRENASD configuration. For those who had not previously analyzed the HIRENASD, this provided a good checkout case for their procedures and parameter selections. We should have done the same thing for the BSCW case. To rectify this, we are making an experimental data set at Mach 0.7 at a lower angle of attack available to analysts. This new benchmark case has transonic flow and oscillating shock, but does not contain separated flow.

## VIII. Acknowledgments

The authors thank and acknowledge the contributions of: the computational teams who contributed to the AePW effort and continue to study these configurations; the AePW organizing committee members who have been instrumental in formulation and conduct of this workshop; Drs. Josef Ballmann, Alexander Boucke and colleagues at RWTH Aachen who contributed the HIRENASD experimental data set; and Dave Piatak of NASA who

contributed the BSCW experimental data set. The authors also thank the NASA Fixed Wing project, the NASA Engineering and Safety Center and the NASA Aeronautical Sciences project for their financial sponsorship.

## IX. References

[1] Burns, Robert, "To a Mouse, on Turning Her Up in Her Nest with the Plough", "Kilmarnock volume," or "Poems, Chiefly in the Scottish Dialect," published by John Wilson, July, 1786, Kilmarnock, Scotland.

[2] "https://c3.nasa.gov/dashlink/projects/47/", January 2013.

[3] Heeg, J.; et al, "Plans for an Aeroelastic Prediction Workshop," IFASD-2011-110, International Forum on Aeroelasticity & Structural Dynamics, June 2011, Paris.

[4] Heeg, J., Chwalowski, P., Florance, J.P., Wieseman, C.D., Schuster, D.M., and Perry, B. III, "Overview of the Aeroelastic Prediction Workshop," AIAA 2013-0783, 51st AIAA Aerospace Sciences Meeting, January 7-10, 2013, Grapevine, Texas.

[5] Schuster, D.M., Heeg, J., Wieseman, C.D., and Chwalowski, P., "Analysis of test case computations and experiments for the Aeroelastic Prediction Workshop," AIAA-2013-0788.

[6] Heeg, J., Chwalowski, P., Wieseman, C.D., Florance, J.P., and Schuster, D.M., "Lessons learned in the selection and development of test cases for the Aeroelastic Prediction Workshop: Rectangular Supercritical Wing," AIAA-2013-0784, 51st AIAA Aerospace Sciences Meeting, January 7-10, 2013, Grapevine, Texas.

[7] Mavriplis, D.J., Yang, Z., and Long, M., and Sitaraman, J., "Results using NSU3D for the First Aeroelastic Prediction Workshop," AIAA 2013-0786, , 51st AIAA Aerospace Sciences Meeting, January 7-10, 2013, Grapevine, Texas.

[8] Raveh, D.E., Yossef, Y.M. and Levy, Y, " Flow simulations for the first Aeroelastic Prediction Workshop using the EZNSS code," AIAA 2013-0787, , 51st AIAA Aerospace Sciences Meeting, January 7-10, 2013, Grapevine, Texas.

[9] Chwalowski, P., Heeg, J., Wieseman, C.D., and Florance, J.P., "FUN3D analyses in support of the First Aeroelastic Prediction Workshop," AIAA 2013-0785, 51st AIAA Aerospace Sciences Meeting, January 7-10, 2013, Grapevine, Texas.

[10] Ballmann, J., Dafnis, A., Korsch, H., Buxel, C., Reimerdes, H.-G., Brakhage, K.-H., Oliver, H., Braun, C., Baars, A., and Boucke, A., "Experimental Analysis of High Reynolds Number Aero-Structural Dynamics in ETW," AIAA Paper 2008-841, Jan.

[11] Ballmann, J., Boucke, A., Dickopp, C., and Reimer, L., "Results of Dynamic Experiments in the HIRENASD Project and Analysis of Observed Unsteady Processes," IFASD Paper 2009-103, June.

[12] Ballmann, J., Dafnis, A., Braun, C., Korsch, H., Reimerdes, H.-G., and Oliver, H., "The HIRENASD Project: High Reynolds Number Aerostructural Dynamics Experiments in the European Transonic Windtunnel (ETW)," ICAS Paper 2006-726, Sept.

[13] Dafnis, A., Korsch, H., Buxel, C., and Reimerdes, H.-G., "Dynamic Response of the HiReNASD Elastic Wing Model under Wind-Off and Wind-On Conditions," Tech. rep., Stockholm, 2007, International Forum on Aeroelasticity and Structural Dynamics, IF-073.

[14] Ballmann, J., et. al., "First Results of the High Reynolds Number Aero-Structural Dynamics (HIRENASD) Experiments in ETW, Keynote lecture at International Forum of Aeroelasticity and Structural Dynamics (IFASD), Stockholm, Sweden, 2007.

[15] Reimer, L., Ballmann, J., Behr, M., "Computational Analysis of High Reynolds Number Aerostructural Dynamics (HIRENASD) Experiments, IFASD-2009-130, Seattle, 22-24 June 2009.

[16] Chwalowski, P., Florance, J., Heeg, J., Wiseman, C., and Perry, B, "Preliminary computational results of HIRENASD configuration in preparation for the Aeroelastic prediction Workshop," IFASD_2011-108, June 2011, Paris.

[17] Neumann, Jens, and Ritter, Markus, "Steady and unsteady aeroelastic simulations of the HIRENASD wind tunnel experiment," IFASD-2009-131, Seattle, 22-24 June 2009.

[18] Neumann, Jens, Nitzsche, Jens, and Voss, Ralph, "Aeroelastic analysis by coupled non-linear time domain simulation," RTO-MP-AVT-154, 2008.

[19] Hassan, David, and Ritter, Markus, "Assessment and prediction capabilities for numerical aeroelasticity based on HIRENASD configuration," IFASD-2011-109, June 2011, Paris.

[20] Schuster, D., Chwalowski, P., Heeg, J., and Wieseman, C., "Summary of data and findings from the First Aeroelastic Prediction Workshop," Tech. rep., Hawaii, 2012, 7th International Conference on Computational Fluid Dynamics, ICCFD7-2012.

[21] Pearcey, H.H., "Some effects of shock-induced separation of turbulent boundary layers in transonic flow past aerofoils," Aeronautical Research Council Reports & Memoranda No 3108, June, 1955.

[22] Heeg, J. and Piatak, D.J., "Experimental data from the Benchmark SuperCritical Wing wind tunnel test on an oscillating turntable," to be presented at the 54th AIAA/ASME/ASCE/AHS/ASC Structures, Structural Dynamics and Materials Conference, April 8-11, 2013 , Boston.

[23] Jirasek, A., Dalenbring, M. et al, "Steady and unsteady investigation of the Benchmark SuperCritical Wing," to be presented at the 55th AIAA Structures, Structural Dyanmics and Materials Conference, April 2013.